Development of the Conditional Moment Closure with a multi-code approach in the frame of Large Eddy Simulations

E. J. Pérez-Sánchez*, D. Mira, O. Lehmkuhl, G. Houzeaux

Barcelona Supercomputing Center (BSC), Edificio Nexus II - C/ Jordi Girona 29, 08034, Barcelona, Spain

Abstract

The Conditional Moment Closure (CMC), devised for turbulent combustion modelling, was implemented in the multiphysics code Alya, based on the Finite Element Method (FEM), in the frame of Large Eddy Simulations (LES) for unstructured meshes. A multi-code approach has been developed to run separately the transport equations for non-reacting variables (CFD) and the conditioned quantities (CMC) in two different meshes. The fundamental aspects of the algorithm are discussed while a new strategy for the interpolation between CFD and CMC meshes is described. The Cambridge swirling burner is analysed and simulations results are compared to measurements.

Introduction

The continuous reduction in pollutant emissions in the energetic and transport sectors, boosted by the national and international regulations, has made of the use of reliable combustion models in practical applications a need. Capturing the plethora of phenomena and interactions appearing in turbulent combustion requires both a model with a rich physical content that allows to apply complex chemical mechanisms as well as the use of High-Performance Computing (HPC) in the frame of Large Eddy Simulations (LES). This is even more important when pursuing extreme reduction of pollutants which many times require moving to conditions where the role of unsteady effects and re-ignition and extinction phenomena are intensified. In this context, several models have been shown to be successful, where the most outstanding results can be mainly grouped in the family of flamelet and Conditional Moment Closure (CMC) models [1, 2].

CMC model was devised to solve turbulent non-premixed flames [3], even it has been extended to premixed combustion [4], by transporting the conditional species mass fractions and enthalpy. In the case of the non-premixed combustion the fields are conditioned to the mixture fraction while in premixed combustion to the progress variable. Now onwards the description will be limited to non-premixed combustion.

Solving conditioned fields implies a high computational cost since it requires to solve the problem in a 4th-dimensional space (x, y, z, η) where η denotes the sample space for mixture fraction. The high computational cost implied by this increase in dimensionality can be palliated by solving the CMC equations in a much coarser mesh than the rest of equations, which will be referred to as the CFD equations. However, defining a proper CMC mesh may still pose some difficulties, usually requires experience and not enough attention has probably been drawn to this aspect in the literature. Therefore, it is considered necessary to focus on such aspect since the accuracy of the simulation may depend to a large extent on the quality of the meshes.

In this paper first a description of the CMC model followed by the implementation of the CMC algorithm in the Alya multiphysics code is described in detail. The algorithm is coded in the context of the Finite Element Method (FEM), which to the authors knowledge, makes of this CMC implementation the first one in the frame of this method. Then, special attention is devoted to the explanation of the new interpolation strategy to transfer information between CMC and CFD meshes. Finally, results with the current implementation are shown for the Cambridge swirling burner [2, 5].

Description of the CMC model

The details of the CMC model can be found in the literature [3] so here the explanation will be limited to the main aspects of the model.

The fundamental idea of CMC is to condition the reacting scalars fields to the mixture fraction in non-premixed combustion as a way to reduce the large fluctuations of such scalars, leading to improved estimations of the chemical source terms. According to the original idea, conditioning implies that the sample space for mixture fraction is divided into a set of bins and for each point in the space (x, y, z) the average values in time for each of the bins are obtained from averaging the part of the reacting scalars signals where the mixture fraction field ξ (note that we distinguish this field from η, which is the sample space for the mixture fraction) shows values between the limits of the corresponding bin. A similar procedure can be adapted to filtering in the context of LES [6]. When the maximum length of the set of bins tends to 0, and after imposing some assumptions, transport equations for the conditional scalars Q_i can be obtained.:

$$\widetilde{\overline{\rho}P}(\eta)\frac{\partial Q_i}{\partial t} + \widetilde{\overline{\rho}P}(\eta)\langle \vec{v} \,|\, \eta\rangle \cdot \nabla Q_i = \nabla(\widetilde{\overline{\rho}P}(\eta)(D + D_{sgs})\nabla Q_i) + \\ + \widetilde{\overline{\rho}P}(\eta)\langle N \,|\, \eta\rangle \frac{\partial^2 Q_i}{\partial \eta^2} + \widetilde{\overline{\rho}P}(\eta)\langle \dot{\omega}_i \,|\, \eta\rangle \tag{1}$$

We denote unconditional filtering by $\langle \cdot \rangle$ while conditioned filtering by $\langle \cdot \,|\, \eta\rangle$ and Favre filtering is applied

* Corresponding author: eduardo.perez@bsc.es

except otherwise stated. In consequence, with this nomenclature $Q_i = \langle Y_i | \eta \rangle$. In eq. (1) the temporal and convective terms can be identified together with the diffusion one, where a gradient hypothesis has been used and the sub-grid mass diffusion is denoted by D_{sgs} to distinguish it from the laminar one D. The term with the second derivative in mixture fraction is a diffusion between mixtures in the CMC space and its intensity is characterized by the conditioned scalar dissipation rate $\langle N | \eta \rangle$. Finally, the chemical source terms closes the equation. Note that multiplying the unconditional Reynolds averaged density $\overline{\rho}$, the filtered probability density function (FPDF) $\widetilde{P}$ appears explicitly in the equation.

The unconditional averages $\langle Y_i \rangle$ are obtained integrating the conditional values Q_i for each point (x, y, z) along the mixture fraction direction. Even there exist alternative methods, the most common is to presume the shape of the FPDF with a beta function, as done in the current work, which is parametrized in terms of the mixture fraction $\langle \xi \rangle$ and its variance $\langle \xi''^2 \rangle$:

$$\langle Y_i \rangle = \int_0^1 Q_i \, \widetilde{P}(\eta; \langle \xi \rangle, \langle \xi''^2 \rangle) \, d\eta \tag{2}$$

$$\widetilde{P}(\eta; \langle \xi \rangle, \langle \xi''^2 \rangle) = \frac{1}{B(a,b)} \eta^{a-1} (1 - \eta^{b-1}) \tag{3}$$

$$a = \langle \xi \rangle \left(\frac{1}{S} - 1 \right); \quad b = (1 - \langle \xi \rangle) \left(\frac{1}{S} - 1 \right) \tag{4}$$

where S is the normalized mixture fraction variance $\langle \xi''^2 \rangle / (\langle \xi \rangle (1 - \langle \xi \rangle))$ and B is the beta function. Mixture fraction and its variance are transported according to:

$$\overline{\rho} \frac{\partial \langle \xi \rangle}{\partial t} + \overline{\rho} \langle \vec{v} \rangle \cdot \nabla \langle \xi \rangle = \nabla (\overline{\rho} (D + D_{sgs}) \nabla \langle \xi \rangle \tag{5}$$

$$\begin{aligned} \overline{\rho} \frac{\partial \langle \xi''^2 \rangle}{\partial t} + \overline{\rho} \langle \vec{v} \rangle \cdot \nabla \langle \xi''^2 \rangle = \\ = \nabla (\overline{\rho} (D + D_t) \nabla \langle \xi''^2 \rangle) + 2 \overline{\rho} D_{sgs} \nabla \langle \xi \rangle \cdot \nabla \langle \xi \rangle - \overline{\rho} N \end{aligned} \tag{6}$$

where the sub-grid part of the scalar dissipation rate N is computed as $2 \langle \xi''^2 \rangle / \tau_t$, where τ_t is a turbulent time scale estimated from the strain tensor, the turbulent viscosity and the average length of the element.

Implementation of the algorithm

CMC has been implemented in Alya, a multiphysics code developed at BSC, based on the FEM which is targeted for massive parallel computation [7]. The implementation is based on a multi-code strategy which relies on MPI (Message Passing Interface) library and consists of two executions for Alya run in parallel [8, 9], one for the CFD where equations (5) and (6) together with continuity and Navier-Stokes are solved, and other for the CMC which integrates equation (1) for all species and computes unconditioned values according to equation (2). Both executions exchange information, namely, $\overline{\rho}$ and laminar viscosity from CMC to CFD and $\langle \xi \rangle, \langle \xi''^2 \rangle, D_{sgs}, \langle \vec{v} \rangle$ and $\langle N \rangle$ from CFD to CMC, at some point of the time step to provide the necessary information to integrate transport equations.

To avoid penalizations in the time step, equation (1) is split into 3 equations:

$$\begin{aligned} \overline{\rho} \widetilde{P}(\eta) \frac{\partial Q_i}{\partial t} + \overline{\rho} \widetilde{P}(\eta) \langle \vec{v} \, | \, \eta \rangle \cdot \nabla Q_i = \\ = \nabla (\overline{\rho} \widetilde{P}(\eta) (D + D_{sgs}) \nabla Q_i) \end{aligned} \tag{7a}$$

$$\frac{\partial Q_i}{\partial t} = \langle N \, | \, \eta \rangle \frac{\partial^2 Q_i}{\partial \eta^2} \tag{7b}$$

$$\frac{\partial Q_i}{\partial t} = \langle \dot{\omega}_i \, | \, \eta \rangle \tag{7c}$$

Notice that equation (7a) is an advection-convection-reaction (ADR) equation which only contains derivatives in the spatial directions and, hence, it can be solved for a constant mixture fraction $\eta = \eta^*$. This means that the 4th-dimensional space (x, y, z, η) can be discretized in different mixture fraction levels $\eta_1, \eta_2 \ldots$ where the mesh in physical space (x, y, z) is repeated at each one. In this way, at each time step equation (7a) is solved for each of the mixture fraction levels η_i, with no exchange of information between mixtures, and later equation (7b), which corresponds to the diffusion between mixture fractions, is solved at each physical node along the mixture fraction direction. As a final step chemistry is integrated through equation (7c) at each physical node and mixture fraction level. This splitting allows to do sub-steps for equations (7b) and (7c), if required, and, hence, not being penalized by the most critical points.

For both equations (7a) and (7b) an explicit Runge-Kutta scheme is applied with order 3 in time and 2 in physical space and mixture fraction while CVODE algorithm from Cantera is used for equation (7c) [10]. Continuity and Navier-Stokes equations, these are solved applying a low-dissipation scheme for low Mach number reacting flows based on the fractional step algorithm with Runge-Kutta third-order temporal scheme [11].

Regarding conditional enthalpy $Q_h = \langle h \, | \, \eta \rangle$, in this work only adiabatic conditions have been considered, hence, Q_h is linearly related to mixture fraction η where values at $\eta = 0$ and 1 are found from the given composition and temperature at the oxidizer and the oxidant, respectively. At any point in the domain and from the values of conditional species mass fractions and enthalpy, conditional temperature is obtained. To obtain the unconditional density with Reynolds filtering, equation (2) is applied to the conditional specific volume and then, the reciprocal is computed. Figure 1 shows graphically the steps followed to solve CMC together with the coupling between codes.

Very extended models have been used for the different terms in equation (1): for velocity is assumed that $\langle \vec{v} \, | \, \eta \rangle = \langle \vec{v} \rangle$ while for $\langle N \, | \, \eta \rangle$ the Amplitude Mapping Closure has been adopted. The sub-grid diffusivity is taken equal for all the mixtures while the laminar diffusivity is computed from the local conditions at each point (x, y, z, η) assuming unity Lewis number. Finally, the conditional chemical source terms are modelled through a first order closure.

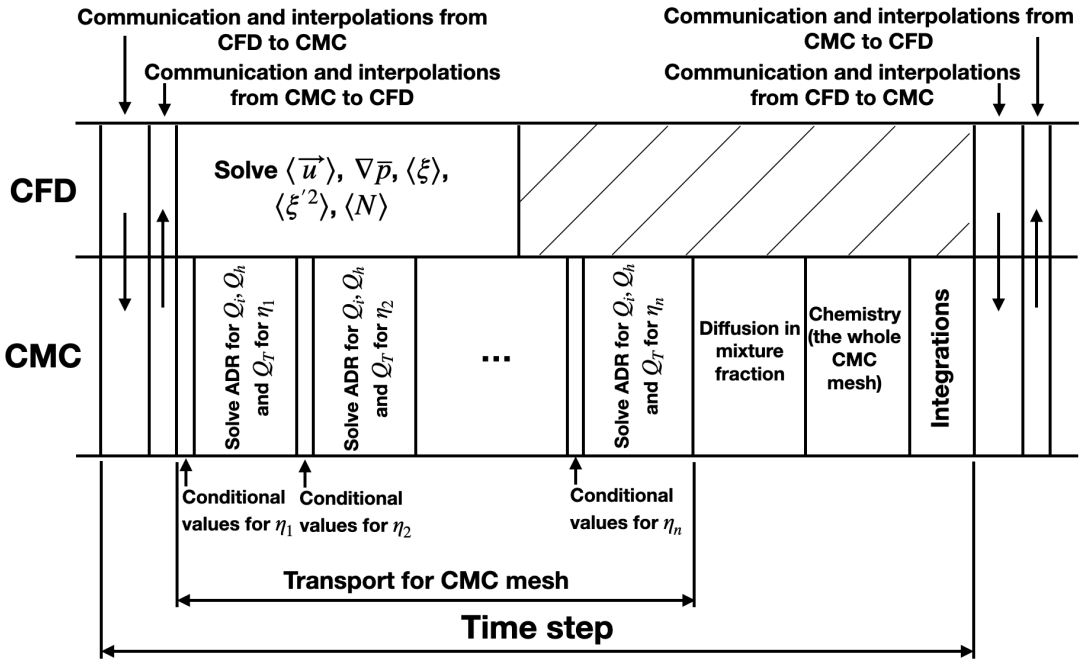

Figure 1: actions to solve one time step. Stripped regions represent idle times.

Mesh interpolation strategy

CMC is a model that involves a high computational cost since the transport equations (7a) have to be solved for the physical mesh as many times as mixture fractions η_i are chosen. Therefore, there is a need of using a coarser mesh for CMC compared to CFD and one of the most abstruse aspects of the model is how to come up with such a mesh. Such coarsening is not only based on reasons of economy but on physical grounds too since conditional fields are expected to show much softer variations than unconditional variables. This statement is in turn a consequence of the smaller fluctuations of the conditional fields claimed in previous section and gives validity to the use of simple closures for the chemical source term, like the first order closure. Many times generating the CMC mesh is done by building it in such a way that each cell contains certain number of complete elements of the CFD mesh or, alternatively, by constructing the CMC mesh and then refining each cell to obtain the CFD mesh, what clearly imposes some limitations. In this paper we present a new strategy, developed in the frame of FEM, which allows total independency between the meshes, that is, nodes do not necessarily coincide and elements of one mesh can be partially contained inside elements of the other mesh.

In general, the transfer of information from CFD to CMC (the transferred fields are those indicated previously) is done through volumetric averages of the conditional fields weighed with the FPDF. In this work, we have considered two types of averages, the first one, is similar to the one explained and we will refer to it as 'Method 1' while the second, which is a simplified method, is computed directly with the unconditional fields and we will call it 'Method 2'. Method 1 and 2 respond to formulae (8) and (9), respectively:

$$\langle \phi \,|\, \eta \rangle^* = \frac{\int_{R_i} \langle \phi \,|\, \eta \rangle \, \widetilde{P}(\eta; \langle \xi \rangle, \langle \xi'^2 \rangle) \, dV}{\int_{R_i} \widetilde{P}(\eta; \langle \xi \rangle, \langle \xi'^2 \rangle) \, dV} \tag{8}$$

$$\langle \phi \rangle^* = \frac{\int_{R_i} \langle \phi \rangle \, dV}{\int_{R_i} dV} \tag{9}$$

Formulae (8) and (9) provide either the conditional or the unconditional value for the transferred fields from CFD to CMC at each of the nodes of the CMC mesh (asterisk is used to denote that the averages are computed in a different mesh to the one used to evaluate the integrands). In the case of $\langle \xi \rangle$ and $\langle \xi'^2 \rangle$ formula (9) has necessarily to be used. The conditional values when using method 2 are obtained applying the models described in previous section to the volumetric averages obtained through formula (9).

Note that, different to what is typically done in the Finite Volume Method (FVM), the integral does not extend to the cell but to a region R_i defined around node i. In this work, such region is composed of the set of elements to which node i belongs to.

Integrals are computed in a similar way as it is typically done in the FEM, that is, through a Gaussian quadrature. However, in order to obtain more representative values, and as many CFD elements may fall inside a CMC element, high order quadrature rules are used for the interpolation between meshes. This implies that two quadrature rules are used in the CMC mesh, one to solve equation (1) and other one, with higher order, for the interpolation from CFD mesh to the CMC one. This procedure allows to use independent meshes for CFD and CMC in the sense that no coincident nodes are required. The geometrical interpretation of the method is schematically represented in figure 2.

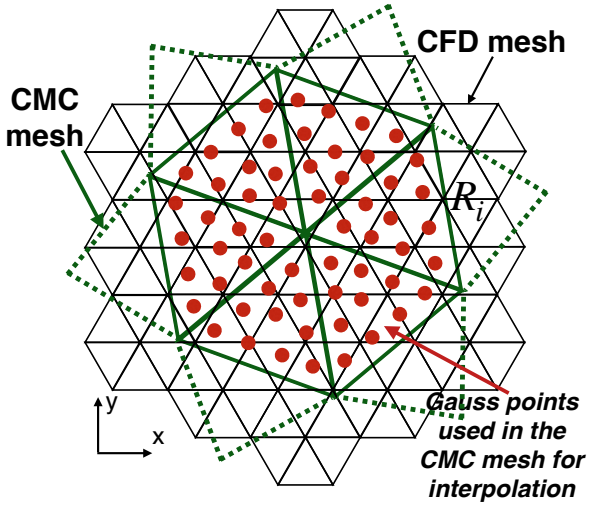

Figure 2: geometrical representation of the interpolation strategy. Elements from CFD mesh are represented in black. Elements from CMC mesh are represented with dashed green lines while the elements of R_i with solid green lines. The Gauss points for the interpolation in the region R_i are marked with red points.

For the transfer of fields from the CMC to the CFD mesh a direct interpolation is used since it is assumed that the discretization in CFD is higher than in CMC.

In the case of having nodes from the CFD mesh outside the CMC one, values are extrapolated taking the value from the nearest CMC node.

Preliminary test

Before analyzing the Cambridge burner, a preliminary test is carried out to study the capabilities of the proposed interpolation strategy. Such test does not correspond to any physical configuration and it is only developed to show the potential of the interpolation.

The CMC model together with the CFD is solved in a one-dimensional problem with an initial mixture fraction and temperature as shown in figure 3. The initial velocity ranges between 0.5 and 1 m/s along the domain and burnt gases are found in the whole domain, which extends 2 cm long. The mechanism used in these simulations is a 19 species and 93 reactions methane scheme generated at BSC [12] through chemistry reduction from GRI3.0 methane mechanism [13]. Three cases have been computed: the reference case where both CFD and CMC meshes are coincident with a total of 500 nodes and two other cases, where the interpolation strategy is applied, with 125 nodes for the CMC mesh. In all the cases the CFD mesh is the same. 59 mixture fraction levels have been used with a refinement around the stoichiometric mixture fraction. Both methods explained previously have been explored in this preliminary test ('Method 1' and 'Method 2' in figure 3).

Results show that an excellent agreement is obtained between the case with coincident meshes and the cases with the interpolation strategy. This has been observed for the species too. Moreover, the influence of the method of interpolation (equations (8) and (9)) does not have any effect on results. Finally, note that the ratio between the number of elements in both cases is 4, implying that in a similar 3D case the ratio would be in the order of $4^3 = 64$, that is, in one CMC element around 65 CFD elements would be found. Hence, the method allows to obtain substantial reductions of the number cells with negligible impact on results. However, in general, the ratio of reduction depends on how fine the CFD mesh, is making difficult providing any number that quantifies the possible reduction even it is expected that noticeable reductions can be achieved.

The Cambridge burner

The experiment simulated in the current work is the Cambridge swirling burner in which a non-premixed flame of methane and air introduced at ambient temperature is burned at atmospheric pressure [5]. Air flows through a six 60º guided vanes diffusor and enters into the combustion chamber after surrounding a bluff-body

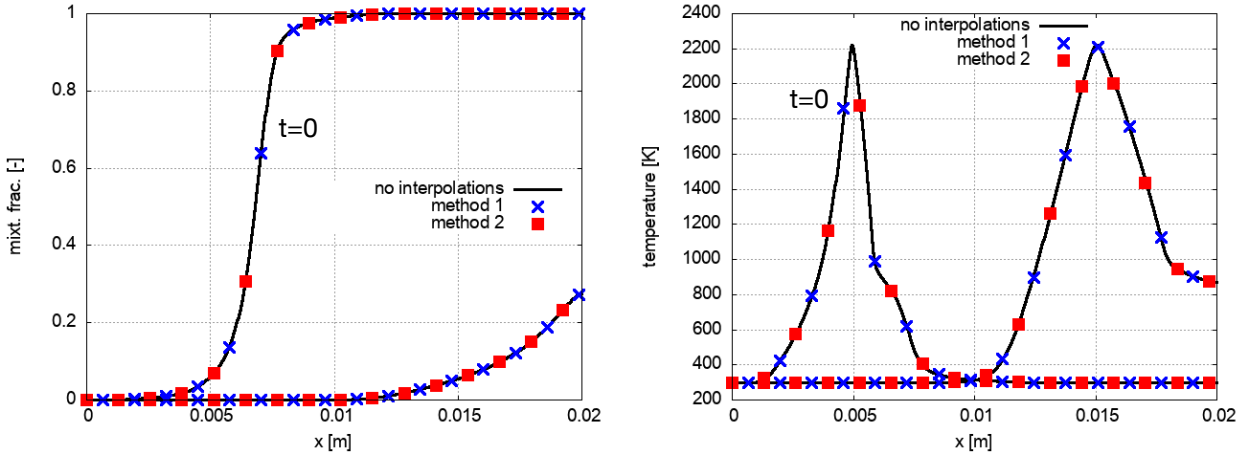

Figure 3: mixture fraction and unconditioned temperature for the validation test. 'No interpolations' is for the case where CFD and CMC meshes are coincident while 'Method 1' and 'Method 2' are both methods explained for the case with interpolations between meshes (equations 8 and 9, respectively).

with a tangential component in the order of 20 m/s which leads to a swirl number of 1.23. The combustion chamber is a parallelepiped with dimensions $0.15 \times 0.095 \times 0.095$ m^3 and fuel is injected through a pipe with an inner diameter of 4 mm and bulk velocity of 29.2 m/s. More details can be found in [2].

Simulations have been carried out for the case of coincident CMC and CFD meshes as well as with different meshes applying the interpolation strategy with both methods. In the case where CFD and CMC meshes are coincident, the mesh is composed of 1.15M nodes and 4M elements with a refinement at the reacting and mixing zones at the entries of the combustion chamber. Cases with interpolations use the same previous CFD mesh but a CMC mesh with 173000 nodes and 1M elements. While in the CFD mesh elements are composed of tetrahedra and prisms in the CMC mesh, in which the mesh in the swirler is coarsened since the flow is inert, only tetrahedral elements have been used. While 4 Gauss points were placed at each CMC element to integrate transport equations in CMC, 15 Gauss points per CMC element were used to compute integrals (8) and (9).

The chemical mechanism used for the preliminary test (19 species, 93 reactions) has been used for these simulations too. As the reference case is very heavy to compute, only 25 mixture fractions, with a higher discretization around the stoichiometric mixture fraction, have been considered. Even in the cases with a reduced CMC mesh it was possible to increase the accuracy of the calculations by refining the mixture fraction mesh, to make a fair comparison with the reference case previous discretization was retained. Moreover, to avoid any possible reflections a buffer layer with a very high viscosity is placed downstream the combustion chamber. For the numerical details see section 'Implementation of the algorithm'.

As a first validation, the mean axial and tangential velocity profiles from simulations are represented and compared to the measurements [5] at different radial cuts in figure 4. For simulations only the averaged velocities for cases with coincident meshes and interpolations with method 1 are represented since very similar results are obtained with method 2. It is observed a very good agreement between the experiments and the simulations what provides a first validation of the CMC model, even some discrepancies are observed in the far field probably caused by considering a too short temporal window for averaging. Moreover, from figure 4 it arises that the use of a coarser mesh in conjunction with the interpolation strategy has not deteriorated the velocity fields.

Figure 5 shows the instantaneous fields for the unconditional scalar dissipation rate, temperature and OH mass fraction. High temperature can be found around stoichiometry accompanied of substantial production of OH, a tracer of high temperature regions. It is interesting to observe how the OH disappears in certain zones (marked with a rectangle in figure 5) as well as temperature falls while an increase in scalar dissipation rate is detected in the same region. In addition, the depletion of OH and reduction of temperature is compensated by an increase in formaldehyde (not shown). This behaviour is attributed to extinction phenomena in agreement with similar conclusions reported in the literature [2, 5].

The results shown so far demonstrate that the current implementation for the CMC model in Alya is correct and the interpolation strategy between meshes, which provides more flexibility compared to the corresponding classical strategies, is appropriate. Hence, these positive conclusions encourage to continue the investigation and apply CMC model to other configurations.

Conclusions

In this work an implementation of the CMC model has been explained in the frame of the FEM targeted for LES simulations. Details regarding the splitting of the different terms have been given in order to not penalize the time step. Special attention has been devoted to the

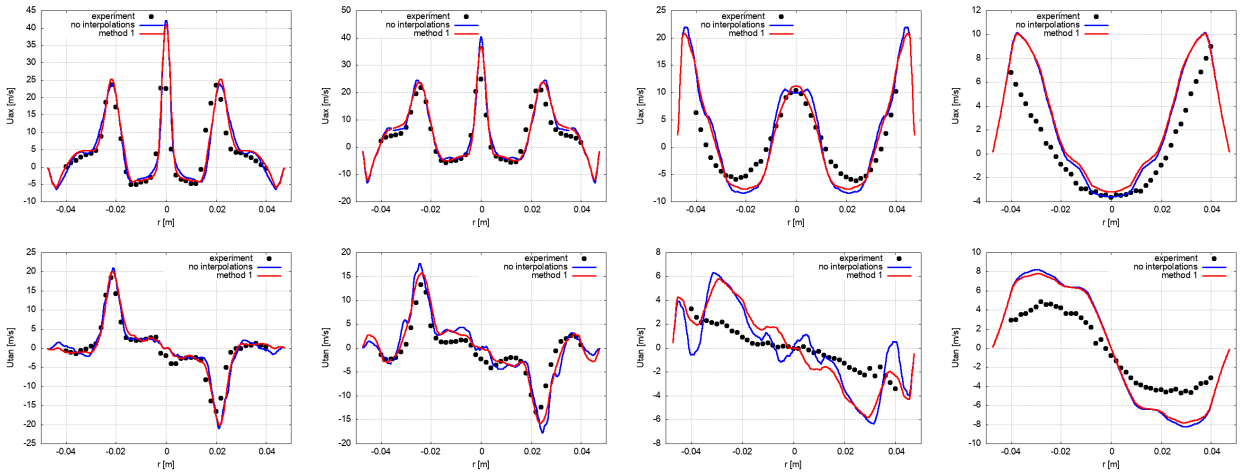

Figure 4: mean axial (top) and tangential (bottom) velocities for the experiment and simulations with coincident CFD and CMC and interpolation strategy with method 1. Radial cuts for distances to the fuel injector of 10 (first column), 15 (second column), 55 (third column) and 110 (fourth column) mm.

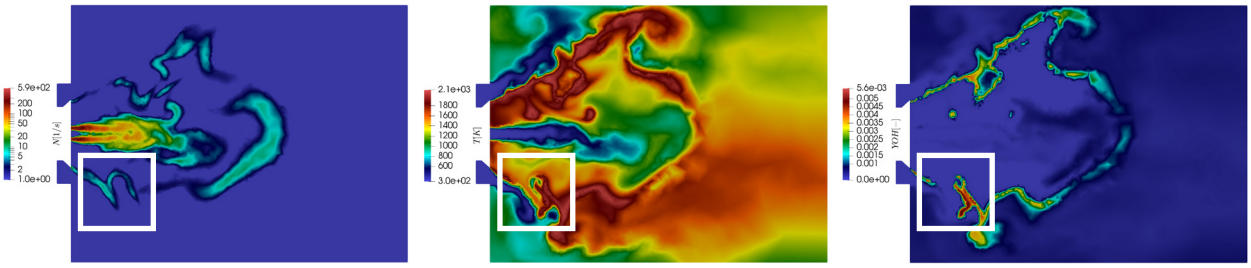

Figure 5: instantaneous unconditional fields for scalar dissipation rate (left), temperature (center) and OH mass fraction (right). Note that a logarithmic scale has been used for the scalar dissipation rate. The rectangle delimits a region where extinction phenomena is observed.

interpolation between CMC and CFD meshes for which a new strategy has been put forward.

First a preliminary test has been explained which has shown very positive results in terms of the interpolations. In a second place, results for the Cambridge burner have been presented for which the interpolation strategy has been applied and compared to the case with very refined mesh for CMC to understand possible losses in the accuracy of results due to the use of coarse meshes for CMC.

Simulations showed very good agreement with experiments as well as almost identical results for the fine and coarse CMC mesh cases. This confirms the suitability of the interpolation strategy. Apart from this, simulations corroborated the apparition of local extinction phenomena as it has been observed in both experiments and numerical studies.

In general terms, the implementation developed for the CMC model shows internal coherence and good agreement with experimental results and this opens the door to continue investigating the CMC model in other configurations as well as extend its capabilities by simulating spray and sooting flames in the frame of FEM.

Acknowledgments

The research leading to these results has received funding from the Clean Sky 2 Joint Undertaking under the European Union's Horizon 2020 research and innovation programme under the ESTiMatE project, grant agreement No 821418.

References

[1] M. Ihme, C.M. Cha, H. Pitsch, Prediction of local extinction and re-ignition effects in non-premixed turbulent combustion using a flamelet/progress variable approach, *P. Combust. Inst.*, 30 (1) (2005) 793-800.

[2] H. Zhang, A. Garmory, D.E. Cavaliere, E. Mastorakos, Large eddy simulation/conditional moment closure modeling of swirl-stabilized non-premixed flames with local extinction, *P. Combust. Inst.*, 35 (2) (2015) 1167-1174.

[3] A. Klimenko, R.W. Bilger, Conditional moment closure for turbulent combustion, *Prog. Energ. Combust.*, 25 (6) (1999) 595-687.

[4] B. Thornber, R.W. Bilger, A.R. Masri, E.R. Hawkes, An algorithm for LES of premixed compressible flows using the Conditional Moment Closure model, *J. Comput. Phys.*, 230(20) (2011) 7687-7705.

[5] D.E. Cavaliere, J. Kariuki, E. Mastorakos, A comparison of the blow-off behaviour of swirl-stabilized premixed, non-premixed and spray flames, F*low Turbul. Combust.*, 91(2) (2013) 347-372.

[6] S. Navarro-Martínez, A. Kronenburg, F. Di Mare, Conditional moment closure for large eddy simulations, *Flow, Turbul. Combust.*, 75(1-4) (2005) 245-274.

[7] M. Vázquez, G. Houzeaux, S. Koric, A. Artigues, J. Aguado-Sierra, R. Arís, D. Mira, H. Calmet, F. Cucchietti, H. Owen, A. Taha, E. Dering Burness, J. M. Cela, M. Valero, Alya: Multiphysics engineering simulation towards exascale, *J. Comput. Sci.*, 14 (2016) 15-27.

[8] J.C. Cajas, G. Houzeaux, M. Vázquez, M. García-Gasulla, E. Casoni, H. Calmet, A. Artigues, R. Borrell, O. Lehmkuhl, D. Pastrana, D.J. Yáñez, R. Pons, J. Martorell, Fluid Structure Interaction based on HPC Multi-Code coupling, *SIAM J. Sci. Comput.*, 40(6) (2018) C677-C703.

[9] G. Houzeaux, M. García-Gasulla, J.C. Cajas, R. Borrell, A. Santiago, C. Moulinec, M. Vázquez, Parallel Multiphysics Coupling: Algorithmics and Computational Performances, *Int. J. CFD*, 34 (7-8) (2020) 1-22.

[10] CANTERA website: https://cantera.org/, 2020

[11] A. Both, O. Lehmkuhl, D. Mira, M. Ortega, Low-dissipation finite element strategy for low Mach number reacting flows, *Comput. Fluids*, 200 (2020), 104436.

[12] A. Surapaneni, Development of a finite rate chemistry solver with tabulated dynamic adaptive chemistry, MSc Thesis TU Delft, http://resolver.tudelft.nl/uuid:667a7a77-fb81-4aca-99db-804cd4c0a516, 2019

[13] G.P. Smith, D.M. Golden, M. Frenklach, N.W. Moriarty, B. Eiteneer, M. Goldenberg, C.T. Bowman, R.K. Hanson, S. Song, W.C. Gardiner, Jr., V.V. Lissianski, Z. Qin, http://www.me.berkeley.edu/gri_mech/, 2020